ELSEVIER

Journal of Fluids and Structures 23 (2007) 463–478

JOURNAL OF FLUIDS AND STRUCTURES

www.elsevier.com/locate/jfs

A consideration on pre- and post-instability of an axisymmetric elastic beam subjected to axial leakage flow

K. Fujita*, H. Morikazu, A. Shintani

Mechanical Systems Engineering, Graduate School of Engineering, Osaka Prefecture University, 1-1, Gakuen-cho, Sakai-City, Osaka Prefecture, 599-8531, Japan

Received 30 July 2004; accepted 12 August 2006
Available online 8 December 2006

Abstract

The dynamical behavior of an axisymmetric elastic beam subjected to axial leakage flow is investigated numerically and experimentally. The coupled equations of motion for a fluid and a beam structure are derived using the Navier–Stokes equation for an axial leakage flow-path and the Euler–Bernoulli beam theory. Performing complex eigenvalue analysis, the variation of the dynamic behavior during pre- and post-instability is investigated with respect to increasing axial leakage flow velocity. Also, an experiment was performed to determine the critical velocity of the unstable dynamic behavior of an axisymmetric elastic beam confined in a concentric cylinder subjected to axial leakage flow through a small annulus, and to measure the variation of the dynamic behavior on pre- and post-instability when the unstable phenomenon with the lower predominant frequency is shifted to the higher one. The relationships between the axial flow velocities and the unstable phenomena are clarified for the transition from the lower mode to the higher mode by comparing the theoretical calculations with experimental observations. Especially, the generation of traveling waves and the energy balance for the distortion of vibration response in the axial direction are discussed and considered at the transition region of the complex coupled vibration response of an axisymmetric elastic beam subjected to an axial leakage flow. Numerical and experimental results are found to be in quite good agreement.

Keywords: Axial leakage flow; Axisymmetric elastic beam; Divergence; Flutter; Stability; Traveling wave; Complex eigenmode

1. Introduction

A fluid is often used as an energy-transfer medium in industrial machines. Also, many machines and structures must be constructed and operated in flowing fluid. The velocities of the fluid are often increased in order to increase the efficiency and make the structural scale more compact. Such increases in velocity sometimes cause a fluid-elastic instability of machines and structures.

In this paper, the fluid-elastic vibration of an axisymmetric circular beam subjected to axial leakage flow is investigated. Examples of such structures include nuclear reactor cores, valves in piping, high-speed trains passing through a tunnel, and robots traveling through the inside of piping.

*Corresponding author.
E-mail address: fujita@mecha.osakafu-u.ac.jp (K. Fujita).

0889-9746/$ - see front matter © 2006 Elsevier Ltd. All rights reserved.
doi:10.1016/j.jfluidstructs.2006.08.016

The vibrational mechanisms of structures subjected to axial leakage flow have been studied by many researchers (Blevins, 1977; Hobson, 1982; Chen, 1987; Yasuo and Païdoussis, 1989; Inada and Hayama, 1990a,b; Païdoussis et al., 1990; Fujita and Ito, 1992; Fujita et al., 1994; Arai and Tajima, 1997; Païdoussis, 1998, 2004). Studies involving an elastic axisymmetric beam and a fluid flow described in terms of the Navier–Stokes equation are however few, although Païdoussis et al. (1990) reported the dynamics and stability of a flexible cylinder using both potential flow theory and an approximate solution of the Navier–Stokes equations for the fluid force acting on the cylinder. The development of improved coupled vibration analysis methodologies, the derivation of the physical meaning of the vibrational characteristics and so on are subjects that remain for future research.

The present authors have already reported on the axial leakage flow-induced vibration of an axisymmetric circular elastic beam based on the Navier–Stokes equation (Fujita and Shintani, 2001). As a continuation of this research, this paper presents an experimental analysis of an elastic beam subjected to axial leakage flow, and describes numerical analyses performed for verification. The variation of mode shape in the vicinity of the critical velocity, and the physical meaning of the occurrence of a traveling wave are investigated experimentally and numerically, and it is shown that there is good agreement between the proposed experiments and theoretical analyses.

2. Theoretical analysis

2.1. Coupled equations and stability analysis

The unstable vibratory behavior of an axisymmetric circular elastic beam shown in Fig. 1(a) is investigated. The elastic circular beam is set coaxially inside of a circular cylinder with a small annular gap H which is assumed to be sufficiently small compared to the radius R and length L of the beam, that is, $H \ll R$, $H \ll L$.

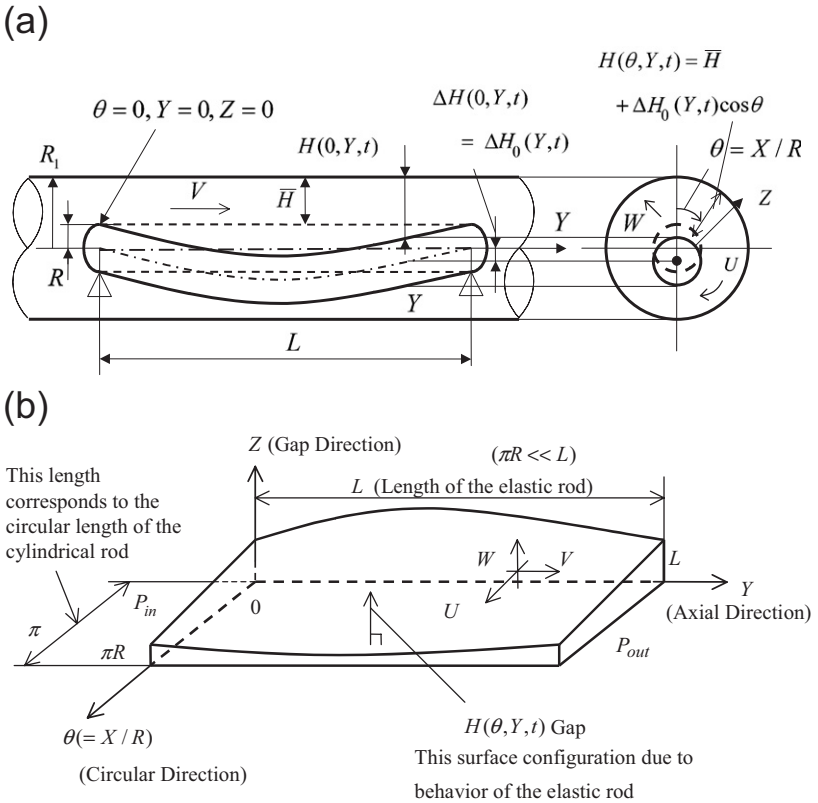

Fig. 1. Analysis model. (a) Axisymmetric elastic beam and axial leakage flow. (b) Expansion of gap to three-dimensional plane from cylindrical coordinate.

As previously mentioned (Fujita and Shintani, 2001), the stability criteria for the leakage flow-induced vibration of an axisymmetric continuous elastic beam with a circular section is obtained by deriving the coupled equation between an elastic beam and an axisymmetric leakage flow, and performing the coupled complex eigenvalue analysis.

The elastic beam is described by the Euler–Bernoulli-type partial differential equation:

$$\rho_s A\frac{\partial^2 \Delta H_0(Y,t)}{\partial t^2}+c_s\frac{\partial \Delta H_0(Y,t)}{\partial t}+EI\frac{\partial^4 \Delta H_0(Y,t)}{\partial Y^4}=\Delta f(Y,t), \tag{1}$$

where ρ_s is the density of the circular beam, A is its cross-sectional area, c_s is the damping coefficient of the beam, $\Delta H_0(Y,t)$ is the small displacement at $\theta=0$ which corresponds to the flexural deflection of the beam, EI is the flexural rigidity of the beam, and $\Delta f(Y,t)$ which is the unsteady force per unit length on the beam,

$$\Delta f(Y,t)=2\int_0^{\pi}\Delta P(\theta,Y,t)R\cos\theta \mathrm{d}\theta, \tag{2}$$

it is calculated by using the unsteady fluid pressure $\Delta P(\theta,Y,t)$, which is described later.

The solution ΔH_0 is assumed to be able to be expanded as a linear combination of the orthonormal modal functions $\{\phi_k(Y)\}$, which are the modes in vacuum (uncoupled modes), as follows:

$$\Delta H_0(Y,t)=\sum_{k=1}^{\infty}\Delta W_k(t)\phi_k(Y), \tag{3}$$

where $\Delta W_k(t)$ is kth time functions.

The axial flow is assumed to be laminar and incompressible. Since the gap is narrow, the annulus is expanded into a three-dimensional Cartesian plane from cylindrical coordinates as shown in Fig. 1(b). The axisymmetric leakage flow is modelled using equations of continuity as the incompressible fluid and momentum based on the Navier–Stokes equations. The following derivation procedure of the unsteady pressure is described in detail in the earlier paper (Fujita and Shintani, 2001). Introducing the flow rates $Q_\theta=\int_0^H U\,\mathrm{d}Z$, $Q_Y=\int_0^H V\,\mathrm{d}Z$, where U and V are the flow velocities in the θ- and Y-directions, and integrating the equations of motion of the fluid, the equations relating pressure, flow rates and gap are obtained. The flow velocity W in the radial direction is assumed to be negligibly small. Dividing the gap, pressure and flow rate into a steady part (denoted with an overbar) and an unsteady part (denoted by $\Delta(\,)$), linearized equations are obtained. Eliminating the flow rates in the resultant equations, the equation of the unsteady pressure is derived.

The unsteady pressure $\Delta P(\theta,Y,t)$ acting on the surface of a circular beam can be obtained by solving the axisymmetric leakage flow based on the Navier–Stokes equations as follows:

$$\Delta P(\theta,Y,t)=\Delta P_0(Y,t)\cos\theta, \tag{4}$$

$$\Delta P_0(Y,t)=-\sum_{k=1}^{\infty}D_{2k}(Y)\frac{\mathrm{d}^2\Delta W_k(t)}{\mathrm{d}t^2}-\sum_{k=1}^{\infty}E_{2k}(Y)\frac{\mathrm{d}\Delta W_k(t)}{\mathrm{d}t}-\sum_{k=1}^{\infty}F_{2k}(Y)\Delta W_k(t), \tag{5}$$

where the functions $D_{2k}(Y)$, $E_{2k}(Y)$ and $F_{2k}(Y)$ depend on the flow velocity and consist of uncoupled eigenfunctions (modal function of the beam in vacuum) $\phi_k(Y)$ and their derivatives, as follows:

$$D_{2k}(Y)=D_{1k}(Y)+\frac{\mathrm{e}^{Y/R}}{\mathrm{e}^{-L/R}-\mathrm{e}^{L/R}}(-\mathrm{e}^{-L/R}D_{1k}(0)+D_{1k}(L))+\frac{\mathrm{e}^{-Y/R}}{\mathrm{e}^{-L/R}-\mathrm{e}^{L/R}}(\mathrm{e}^{L/R}D_{1k}(0)-D_{1k}(L)), \tag{6}$$

$$E_{2k}(Y)=E_{1k}(Y)+\frac{\mathrm{e}^{Y/R}}{\mathrm{e}^{-L/R}-\mathrm{e}^{L/R}}(-\mathrm{e}^{-L/R}E_{1k}(0)+E_{1k}(L))+\frac{\mathrm{e}^{-Y/R}}{\mathrm{e}^{-L/R}-\mathrm{e}^{L/R}}(\mathrm{e}^{L/R}E_{1k}(0)-E_{1k}(L)), \tag{7}$$

$$\begin{aligned}F_{2k}(Y)=F_{1k}(Y)&+\frac{\mathrm{e}^{Y/R}}{\mathrm{e}^{-L/R}-\mathrm{e}^{L/R}}\left(-\mathrm{e}^{-L/R}F_{1k}(0)+F_{1k}(L)-\mathrm{e}^{-L/R}\frac{\xi_{\mathrm{in}}\rho\bar{Q}_Y^2}{\bar{H}^3}\phi_k(0)-\frac{\xi_{\mathrm{out}}\rho\bar{Q}_Y^2}{\bar{H}^3}\phi_k(L)\right)\\&+\frac{\mathrm{e}^{-Y/R}}{\mathrm{e}^{-L/R}-\mathrm{e}^{L/R}}\left(\mathrm{e}^{L/R}F_{1k}(0)-F_{1k}(L)+\mathrm{e}^{L/R}\frac{\xi_{\mathrm{in}}\rho\bar{Q}_Y^2}{\bar{H}^3}\phi_k(0)+\frac{\xi_{\mathrm{out}}\rho\bar{Q}_Y^2}{\bar{H}^3}\phi_k(L)\right),\end{aligned} \tag{8}$$

with the functions $D_{1k}(Y)$, $E_{1k}(Y)$, $F_{1k}(Y)$ as follows:

$$D_{1k}(Y)=\frac{\rho R^2}{1-R^4 b\lambda_k}\left\{\frac{1}{\bar{H}}\phi_k(Y)+\frac{R^2}{\bar{H}}\frac{\mathrm{d}^2\phi_k(Y)}{\mathrm{d}Y^2}\right\}, \tag{9}$$

$$E_{1k}(Y)=\frac{\rho R^2}{1-R^4 b\lambda_k}\left\{\frac{12v}{\bar{H}^3}\phi_k(Y)+\frac{2\bar{Q}_Y}{\bar{H}^2}\frac{\mathrm{d}\phi_k(Y)}{\mathrm{d}Y}+\frac{12vR^2}{\bar{H}^3}\frac{\mathrm{d}^2\phi_k(Y)}{\mathrm{d}Y^2}+\frac{2\bar{Q}_Y R^2}{\bar{H}^2}\frac{\mathrm{d}^3\phi_k(Y)}{\mathrm{d}Y^3}\right\}, \tag{10}$$

$$F_{1k}(Y)=\frac{\rho R^2}{1-R^4 b\lambda_k}\left\{\frac{\bar{Q}_Y^2 b\lambda_k R^2}{\bar{H}^3}\phi_k(Y)+\frac{36v\bar{Q}_Y}{\bar{H}^4}\frac{\mathrm{d}\phi_k(Y)}{\mathrm{d}Y}+\frac{\bar{Q}_Y^2}{\bar{H}^3}\frac{\mathrm{d}^2\phi_k(Y)}{\mathrm{d}Y^2}+\frac{36v\bar{Q}_Y R^2}{\bar{H}^4}\frac{\mathrm{d}^3\phi_k(Y)}{\mathrm{d}Y^3}\right\}, \tag{11}$$

and the parameters $b=\rho_s A/EI$, $\lambda_k=\omega_k^2$, with ω_k being the eigenfrequency of the beam in a vacuum.

Finally, the coupled equations of motion considering fluid-structure interaction can be derived in the following matrix form:

$$[M_s+M_a]\frac{\mathrm{d}^2}{\mathrm{d}t^2}\{W_n(t)\}+[C_s+C_a]\frac{\mathrm{d}}{\mathrm{d}t}\{W_n(t)\}+[K_s+K_a]\{W_n(t)\}=\{0\}, \tag{12}$$

where $\{W_n(t)\}=\{\Delta W_1(t),\Delta W_2(t),\ldots,\Delta W_n(t)\}^{\mathrm{T}}$ is the modal vector when the mode number is truncated at n, and the coefficient matrices $[M_s]$, $[C_s]$ and $[K_s]$ represent the modal mass, damping and stiffness matrices of the elastic beam, respectively. $[M_a]$, $[C_a]$ and $[K_a]$ are the added mass, added damping, and added stiffness matrices, respectively, describing fluid-structure interaction, and depend on the flow velocity $\bar{V}=\bar{Q}_Y/\bar{H}$.

Let us represent Eq. (12) in state space. The state vector is introduced as $\{z(t)\}=\{W_n^{\mathrm{T}}(t)\ \ \dot{W}_n^{\mathrm{T}}(t)\}^{\mathrm{T}}$ and the following matrix is obtained:

$$[A]=\begin{bmatrix}[O_n] & [I_n]\\ -[M_g]^{-1}[K_g] & -[M_g]^{-1}[C_g]\end{bmatrix}, \tag{13}$$

where $[M_g]=[M_s+M_a]$, $[C_g]=[C_s+C_a]$, $[K_g]=[K_s+K_a]$, and $[I_n]$ and $[O_n]$ are the unit and zero matrices. The coupled equation is then rewritten as

$$\{\dot{z}(t)\}=[A]\{z(t)\}. \tag{14}$$

By analysis of the coupled eigenvalue (complex eigenvalue) s of the matrix $[A]$, the stability of the coupled system can be investigated. In the following calculations, the Software MATLAB is used to calculate the eigenvalues. The root-locus (Argand) diagram can be obtained by complex-analysis of Eq. (13) corresponding to the flow velocity $\bar{V}$ and by plotting the real and imaginary parts of the eigenvalue s. An imaginary part of the complex eigenvalue s, $\mathscr{I}m(s)\neq 0$ and a real part $\mathscr{R}e(s)>0$ implies a dynamic instability (flutter), and $\mathscr{I}m(s)=0$ and $\mathscr{R}e(s)>0$ implies a static instability (divergence).

Therefore, the coupled jth complex eigenmode $\phi_j^c(Y)$ is then expressed as follows:

$$\phi_j^c(Y)=\sum_{i=1}^{n}\phi_i(Y)\psi_{ji}, \tag{15}$$

where $\{\psi_{ji}\}$ is determined by the complex vector $\{Z\}$.

Thus, the critical flow velocity and coupled vibration modes for the leakage flow-induced vibration can be evaluated by this process.

2.2. Accuracy of the proposed method

As a numerical example, the external cylinder is considered to be rigid and the flexible hollow rod to be made of polyvinyl chloride (PVC), and water in the annulus is used as the fluid in this subsection. The dimensions of the model are given by length $L=1000\,\mathrm{mm}$, outer and inner radius of the rod $R=10\,\mathrm{mm}$, $R_{\mathrm{in}}=7\,\mathrm{mm}$ and the gap width $\bar{H}=1\,\mathrm{mm}$. At first, the rod is assumed to be simply supported at both ends.

Here, let us consider how the number of eigenmodes in a vacuum (the number of comparison functions) affects the accuracy of coupled complex modes. In Fig. 2, the relation between the number of comparison functions employed to calculate the complex eigenvalues and the absolute values of first–third complex eigenvalues before and after instability is shown using the dimensions described above. As the axial velocity becomes high, more modes are necessary for keeping the same accuracy. It can be said that the coupled modes almost converge when more than the first 10 comparison functions are used. Though this accuracy depends on the dimensions of the model, it can be considered to be all right for similar dimensions as used in this figure. From the above viewpoint, the number of comparison functions

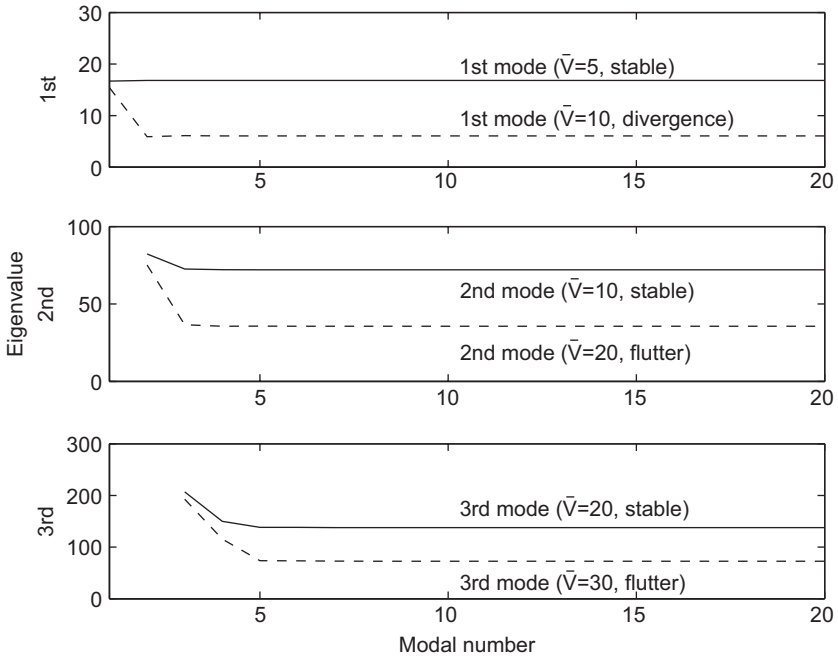

Fig. 2. Relation among number of eigenmodes in a vacuum (comparison functions) for several axial flow velocities and the accuracy of the calculated complex eigenvalues.

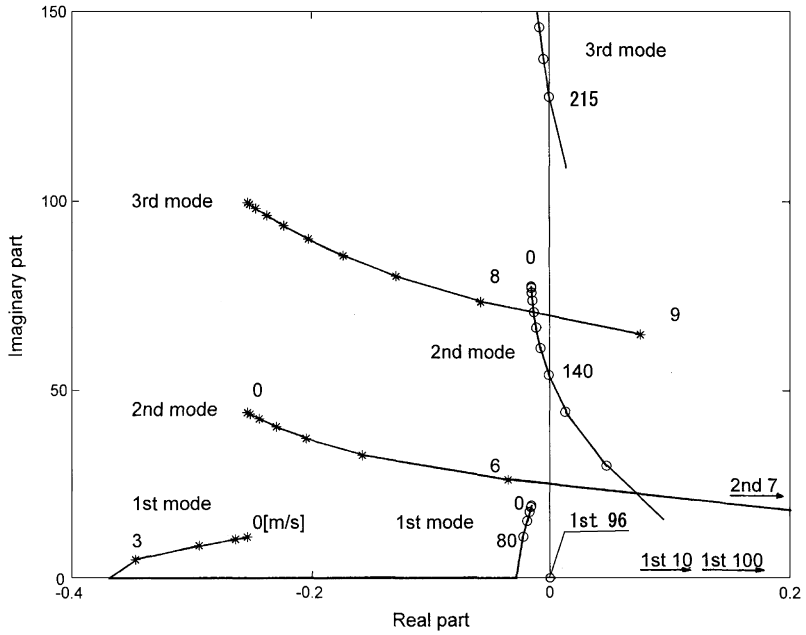

Fig. 3. Effect of fluid characteristics on stability of a simply supported beam: ○, air; ✻, water; $\bar{H} = 4\,\text{mm}$, $E = 9.44 \times 10^7\,\text{Pa}$, $L = 0.8\,\text{m}$, $2R = 16\,\text{mm}$.

is set as $n = 10$ in the following calculations. In Païdoussis (1998), the number of modes $N = 3, 4$ is considered to be adequate for predicting the critical velocity. Therefore, the result examined in Fig. 2 can be said to be reliable and practical.

2.3. Root-locus (Argand) diagram

Let us present the theoretical results based on the above-mentioned theory (Fujita and Shintani, 2001) before the experimental analysis is explained. Fig. 3 shows the root-locus (Argand) diagram of a simply supported elastic beam, as determined by the complex eigenvalue analysis for air and water. The length of the beam is $L = 0.8\,\mathrm{m}$, with outer radius of $R = 8\,\mathrm{mm}$, gap width of $\bar{H} = 4\,\mathrm{mm}$, and Young's modulus of $E = 9.44 \times 10^7\,\mathrm{Pa}$. These dimensions also apply to the experimental model. As the flow velocity increases, the first mode becomes unstable, eventually giving rise to divergence, whereas the second and third modes lead to flutter. The vibration in air is found to be more stable than in water.

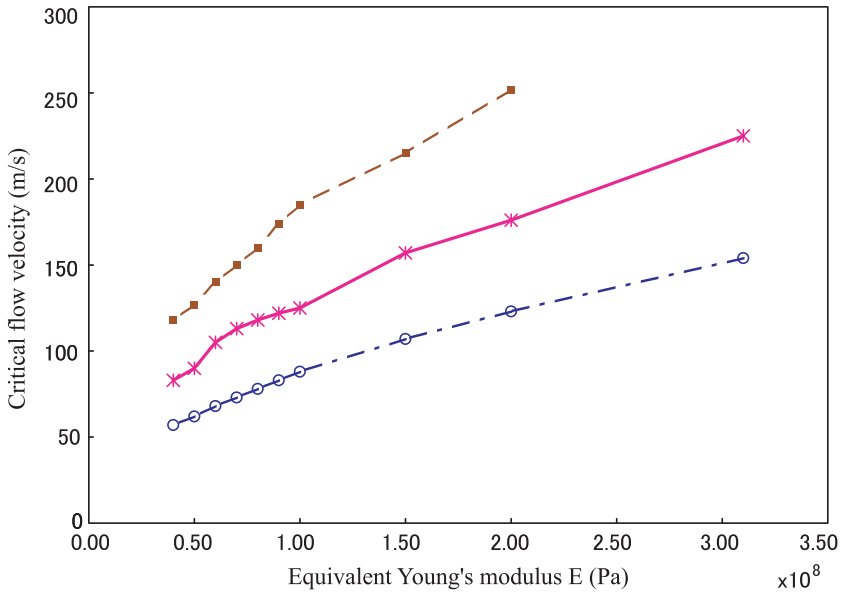

Fig. 4. Influence of the Young's modulus of a beam on the critical flow velocity: ○, first mode; ✳, second mode; ■, third mode; air; $L = 0.8\,\mathrm{m}$, $2R = 16\,\mathrm{mm}$, $\bar{H} = 3\,\mathrm{mm}$.

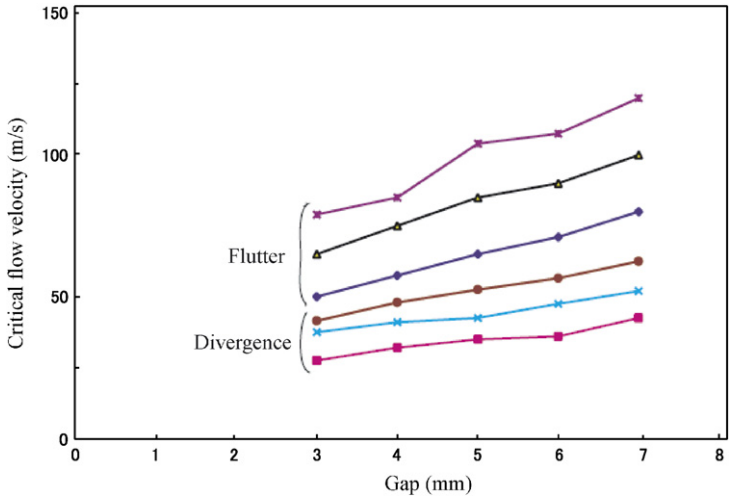

Fig. 5. Influence of gap and length on the critical flow velocity: from the upper curve, $L = 1.0\,\mathrm{m}$ flutter; $L = 1.2\,\mathrm{m}$ flutter; $L = 1.5\,\mathrm{m}$ flutter; $L = 1.0\,\mathrm{m}$ divergence; $L = 1.2\,\mathrm{m}$ divergence; $L = 1.5\,\mathrm{m}$ divergence; air; $E = 3.07 \times 10^7\,\mathrm{Pa}$, $2R = 16\,\mathrm{mm}$.

2.4. Effect of dimensions of an elastic beam model on stability

We investigated the vibrational characteristics and the unstable phenomena by performing parametric studies by varying the flow velocity, the length of the experimental beam model, the gap size between the outer radius of the elastic beam model and the inner radius of the circular cylinder, the density, and the equivalent Young's modulus of the elastic beam model. Fig. 4 shows the relation between the equivalent Young's modulus of an elastic beam and the critical velocity. It is found that the critical flow velocity becomes lower when the elasticity of the beam is lower.

Fig. 5 shows the influence of the length of the beam and of the annular gap on the critical flow velocity. The vibration is found to become unstable at smaller flow velocity as the annular gap is reduced and the length is increased.

3. Experiment and comparison with theory

3.1. Test apparatus

Fig. 6 shows the apparatus used to examine the axial leakage flow vibration of an axisymmetric elastic beam. The axisymmetric circular elastic beam is made of silicone rubber, and a brass wire is inserted down this center in order to maintain straightness and to tune the natural frequency as shown in Fig. 7(a). The simply supported boundary condition is realized by simply-fixing the wire at the center of the outer cylinder on both ends as shown in Fig. 7(b). The inlet and outlet are tapered to suppress turbulence due to flow separation, as shown in Fig. 7(c).

Fig. 8 shows the experimental instrumentation system. The vibration of the beam was measured by using a laser measurement system in order to avoid any possible deterioration of accuracy due to contact measurement. Specification of the laser sensor is as follows. The normal distance for measurement is 30 mm. The range of measurement is ±5 mm. The resolution of the laser sensor is 1 μm and the sampling period is 512 μs. Axial flow was driven by a blower operating in suction mode, which was installed at the outlet of the flow channel to suppress the influence of turbulence due to flow separation. The overall signals detected by the laser sensors were analyzed by using a FFT analyzer. The random noise due to flow turbulence was eliminated by ensemble averaging procedures. Further, the vibration mode shapes were measured and determined by both the analyzed data based on FFT and high-speed photographs.

3.2. Experimental model and preliminary analysis

Table 1 shows the dimensions of the experimental model. The length of the beam is 0.8 m, the diameter 16 mm, the inner diameter of the outer cylinder 24 mm, hence the gap width is 8 mm. It is difficult to set the elastic beam in the center of a narrow passage. Hence, the gap came to be a little larger, although the larger gaps reduce the accuracy of the theory presented. The beam model is simply supported at both ends. The equivalent Young's modulus of the silicone rubber beam is 9.44×10^7 Pa; it was measured exactly by performing a free vibration test.

In the experiment, air is used as the fluid such that the root-locus (Argand) diagram of the experimental model corresponds to the case shown in Fig. 3 for air-flow. The first vibrational mode develops divergence instability at an axial leakage flow velocity of 96 m/s, followed by flutter instability in the second mode at 140 m/s, as shown by the root-locus diagram in Fig. 3. This dynamical behavior agrees with what was observed by Païdoussis (2004) for essentially unconfined flow.

The coupled mode is assumed by the linear combination of uncoupled modes as shown in Eq. (15). Hence the ψ_{ji} is the complex number ratio of the ith uncoupled mode content in the jth coupled mode. Moreover, Fig. 9 shows the relation between the flow velocity and the ratio $\sum_{i(i\neq j)}^{n}(|\psi_{ji}|/|\psi_{jj}|)$ of the jth uncoupled vibrational mode and other uncoupled modes included in the jth coupled mode. $\sum_{i(i\neq j)}^{n}(|\psi_{ji}|/|\psi_{jj}|) \simeq 0$ implies $\phi_j^c(Y) \simeq \phi_j(Y)\psi_{jj}$, that is, the jth coupled mode is almost the jth uncoupled mode. In case of a still fluid, this relation holds. Focusing on the second mode for the velocity $\bar{V} = 215$ m/s before the onset of flutter of the third mode, the ratio of the modes except the second uncoupled mode included in the second coupled mode $\sum_{i(i\neq 2)}^{n}(|\psi_{2i}|/|\psi_{22}|)$ changes rapidly. Then the second coupled mode shape changes rapidly with increasing velocity. This is related to the generation of the traveling wave in the theory, as described later.

3.3. Experimental results and comparison with theory

Although the theory presented is linear, it is applied in the post-critical domain, as the geometric nonlinear effects cannot be considered to be predominant because the gap between the inner beam and the outer rigid cylinder is

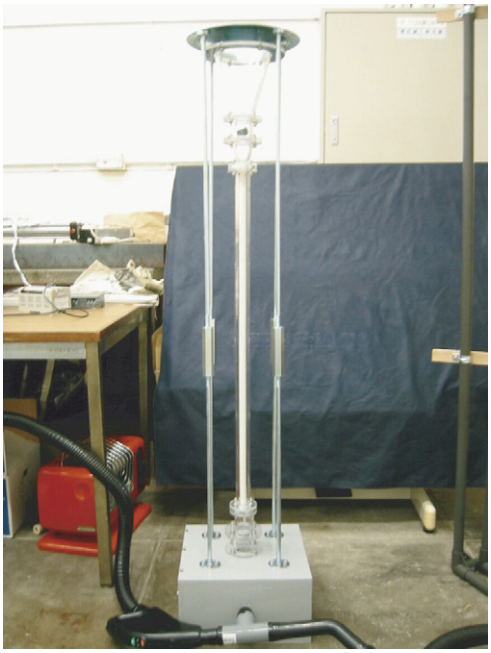

Fig. 6. Test apparatus for axial leakage flow-induced vibration of an axisymmetric elastic beam.

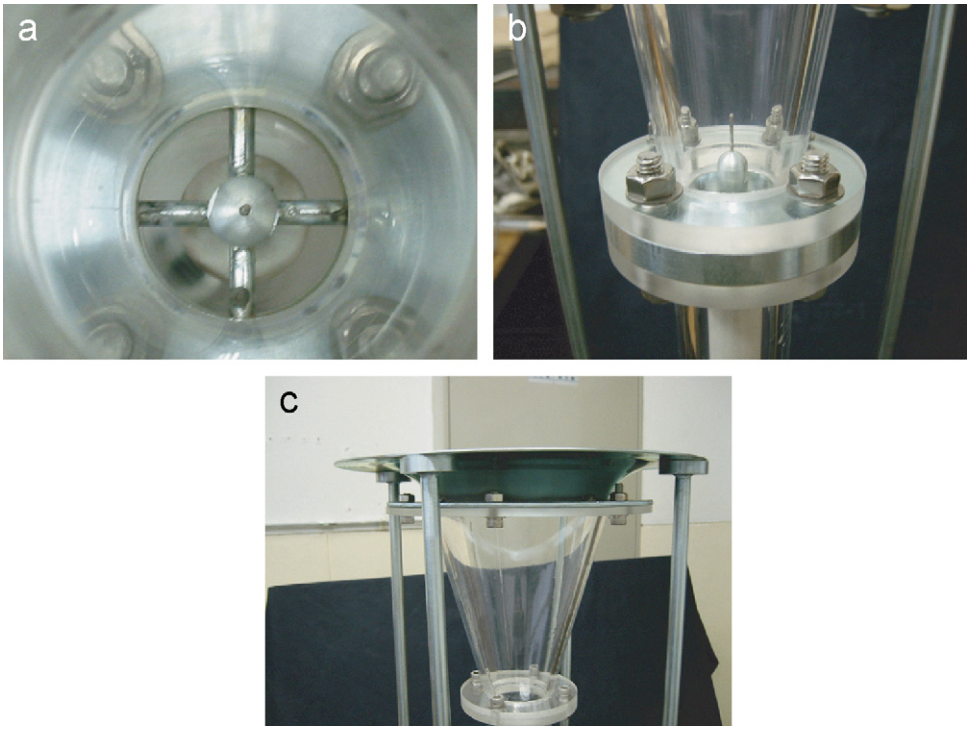

Fig. 7. Detailed composition of the test apparatus. (a) Brass wire installed at the center of the outer cylinder. (b) Simply fixing a brass wire at the inlet and outlet portions. (c) Taper shape nozzle at the inlet portion.

relatively small compared with other dimensions. With increasing axial flow velocity, divergence was recognized first in the experiment, followed by flutter, in good agreement with the numerical results. Table 2 shows a comparison between the critical velocities determined by experiment and theory, respectively.

Fig. 10 shows the comparison between experimental and calculated critical velocity. Moreover, the onsets of divergence and flutter are illustrated simultaneously in this figure, and the onset of a traveling wave (which is explained later more concretely) is also illustrated here.

Table 2 and Fig. 10 show that there is good agreement between the experimental results and theoretical analysis. In addition, the slight difference between the critical velocities of the third mode is considered to be due to the assumption of laminar flow and the omission of compressibility in the theory.

Fig. 11 shows the variation in mode shape for both the experiment and the theoretical analysis with increasing flow velocity. The vibrational characteristics can be classified from this figure into the following 10 steps with primary reference to the experimental results:

1. First mode vibration with small amplitude in the experiment.
2. First mode vibration with slightly larger amplitude in the experiment.
3. Divergence of the first mode appears in the experiment (86.25 m/s) and theory (96 m/s), and the position of the maximum amplitude is shifted slightly downstream in both experiment and theory.
4. After the beam contacts the inner surface of the cylinder due to first mode divergence, the remainder of the beam begins vibrating in the experiment.
5. First mode divergence is distorted in the theory and flutter of the second mode appears in the experiment (148 m/s) and theory (140 m/s).

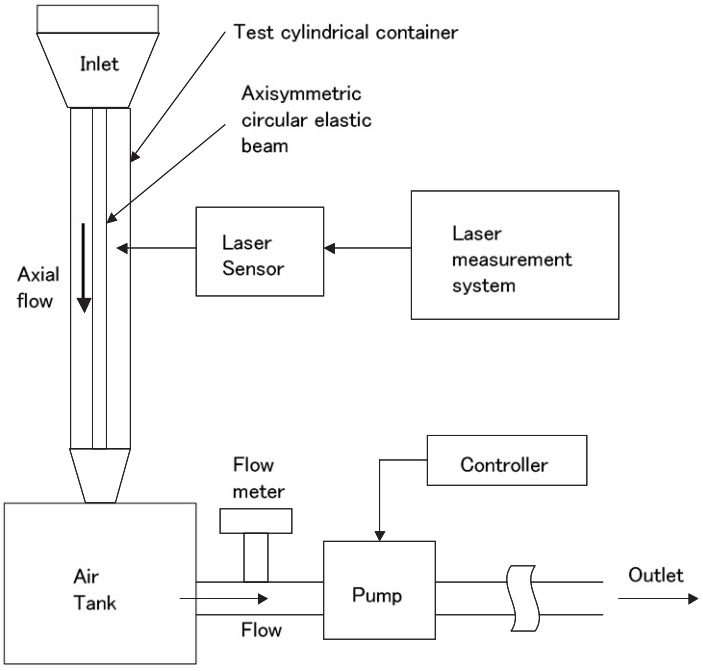

Fig. 8. Experimental instrument system measuring the axial leakage flow-induced vibration of a beam.

Table 1
Dimensions of an experimental model

Length of beam	0.8 m
Diameter of beam	16 mm
Equivalent Young's modulus of beam	9.44×10^7 Pa
Inner diameter of outer cylinder	24 mm

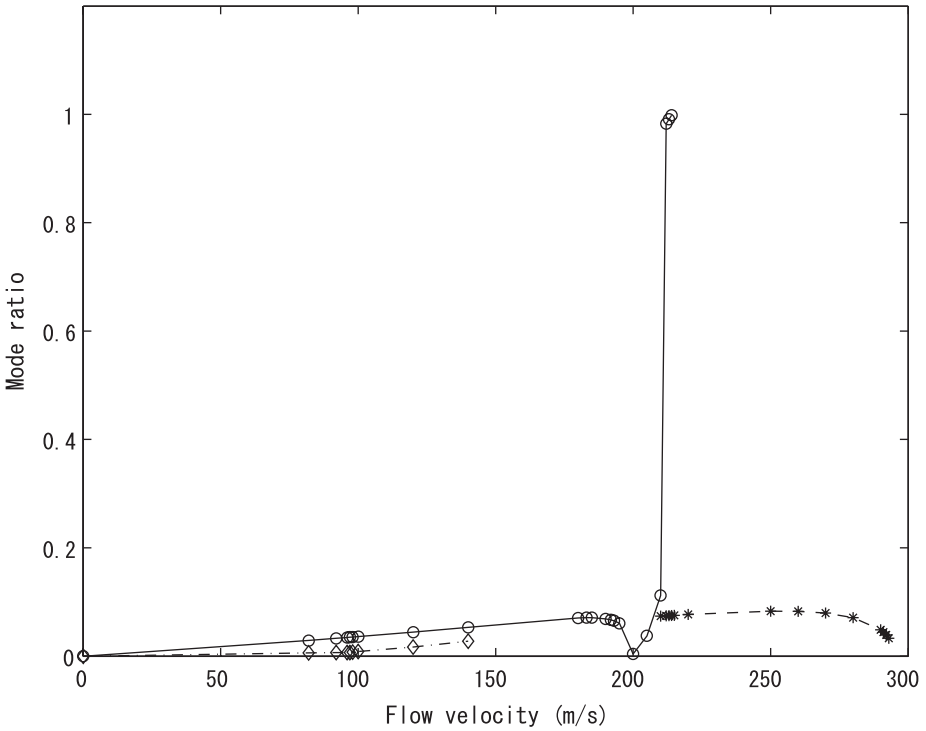

Fig. 9. Relation between the flow velocity and the ratios of the special uncoupled mode and other modes included in the coupled mode: ◇, ratio of the first uncoupled and other uncoupled modes included in the first coupled mode; ○, ratio of the second uncoupled and other uncoupled modes included in the second coupled mode; ∗, ratio of the third uncoupled and other uncoupled modes included in the third coupled mode.

Table 2
Comparison between experimental and calculated critical velocity

	Experimental value (m/s)	Theoretical value (m/s)	Relative error [(exp-theor)/theor]
1st	86.25	96	−0.102
2nd	148	140	0.0571
3rd	170	215	−0.209

6. Divergence of the second mode appears in the experiment (about 162 m/s) and theory (about 195 m/s).
7. After the beam contacts the inner surface of the cylinder due to second mode divergence, the remainder of the beam begins vibrating in the experiment.
8. The vibrational amplitude of the downstream portion becomes larger due to the onset of a traveling wave in the experiment (about 165 m/s) and theory (about 200 m/s).
9. A traveling wave is observed in both experiment and theory.
10. Flutter of the third mode appears in the experiment (170 m/s) and theory (215 m/s).

The traveling wave is identified in the theoretical analysis if the axial position with maximum amplitude of the mode moves in the axial direction during one period due to phase lags among the modes in vacuum. This corresponds to the rapid change of the mode ratio of the referred uncoupled mode and other uncoupled modes shown in Fig. 9. It is found that two types of flutter, namely the flutter not accompanying the traveling wave (Step 5) and the flutter accompanying traveling wave (Step 8) in Fig. 11 exist. As a whole, the theory is considered to reproduce vibration phenomena well, except for nonlinear behavior in the experiment due to impact between the beam and the inner surface of the cylinder. Besides, for the air flow at 20 °C and atmospheric pressure, the onset of divergence at a mean flow speed $\bar{V} = 96\,\mathrm{m/s}$

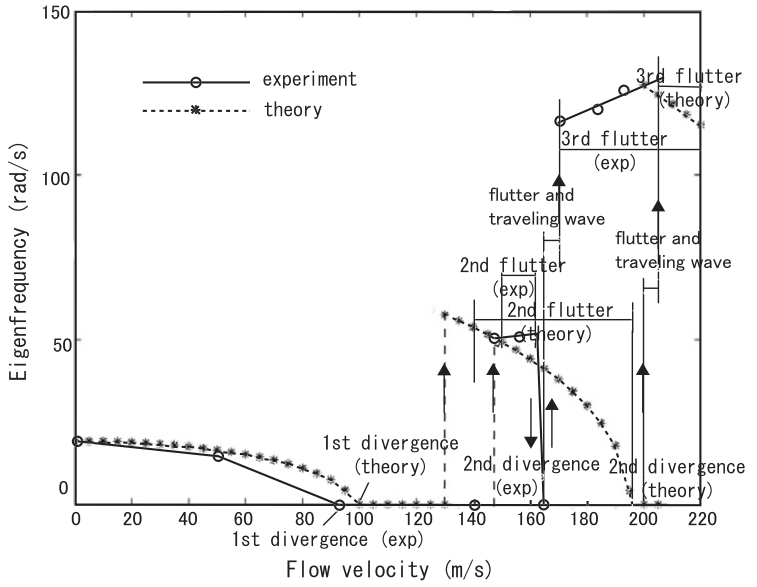

Fig. 10. Comparison between experimental and calculated critical velocity: ○, experiment; ∗, theory.

using a kinematic viscosity $v = 1.5 \times 10^{-5}\,\mathrm{m^2/s}$ is in the turbulent flow region. Also, the Mach number at the onset of divergence is $M = \bar{V}/c = 0.28$ using the speed of sound $c = 340\,\mathrm{m/s}$, that is on the limit that compressibility effects can be ignored. Therefore, as the theory adopted in this paper is based on laminar flow, the numerical calculation results may be predicted to be qualitative, not quantitative for evaluating the dynamic pre- and post-instability behavior. However, the comparison between experimental and theoretical results shows that the linear theory is capable of providing estimates sufficiently accurate for many engineering purposes.

Fig. 12 compares the experimental and simulated traveling components of the second mode shape over one period. The arrows indicate the position of the maximum vibrational amplitude. The traveling wave is identified also in the experiment since the axial position with maximum amplitude of the vibration is observed to move in the axial direction during one period. Again, the results are in good agreement.

Fig. 13 shows photographs of the traveling third mode shape over one period observed in the experiments. Similarly to the second mode in Fig. 12, the axial position with maximum amplitude of the vibration is also observed to move in the axial direction during one period.

4. Discussion

4.1. Comparison between experiments and theory

In the experiment, we employed the elastic beam with low stiffness to obtain the divergence and flutter easily. However, when we reduced the gap, the experimental model contacted the inner side of rigid cylinder because the straightness of the beam could not be maintained well. Therefore, we adopted the brass wire inserted in the center of the beam to keep the straightness. Yet, it is still difficult to set such an elastic beam in a very narrow passage in the experiment, which would satisfy perfectly the assumption of $H/R \ll 1$, $H/L \ll 1$ in our proposed theory. Hence, we could find no other way except for adopting a little wider gap. In spite of these difficulties, an attempt is made to clarify the dynamics of an axisymmetric elastic beam subjected to an axial leakage flow at the pre- and post-instability.

From Figs. 10 and 11, the theoretical results by the complex eigenvalue analysis using the Navier–Stokes equation in an axial leakage flow-path and the Euler–Bernoulli beam theory appear to agree well with the experimental results in terms of the critical velocity and distortion of the vibration response at the transition from the lower mode to the higher mode. However, some differences between the experiments and theory can be seen for the higher modes, possibly due to the assumption of laminar flow and the omission of compressibility of the fluid in the theory.

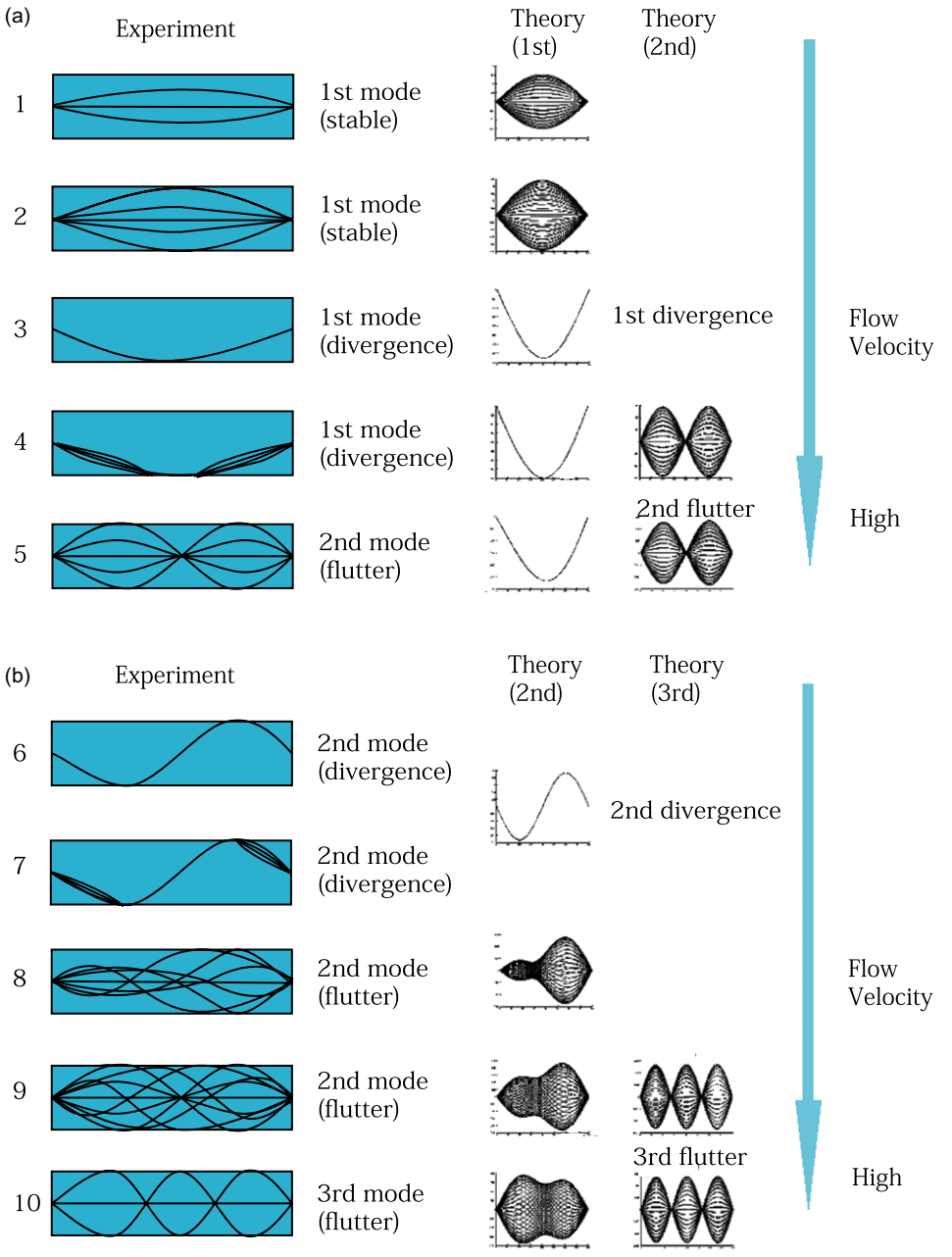

Fig. 11. Comparison of variation in vibrational mode shape between the experiment and the theory with increasing flow velocity. (a) Transition from first mode to second mode. (b) Transition from second mode to third mode.

4.2. *Coupled vibrational modes and traveling waves*

Based on the present results, the predominant unstable vibration of a beam subjected to axial leakage flow appears to shift from the coupled first mode to the second mode, and then to the third mode. When the lower mode is shifted to the higher mode, the symmetry and asymmetry between the upstream and downstream parts of the vibration modes collapse and the vibration response becomes distorted. The onset of this distortion of the coupled mode shape causes the first mode to shift to the second mode, and then the second mode to shift to the third mode. In particular, from the

flutter of the second coupled mode to the third coupled mode observed in theory, the nodal point of the mode shape begins to travel after the distortion appears. Generally speaking, the nth flutter can be said to be unable to shift to the $(n+1)$th flutter until a traveling wave has been generated, except for the first coupled mode. This mechanism of a traveling wave generation is summarized in Fig. 14. The fact that flutter and traveling wave is not the same thing is understood to exist in this study experimentally and analytically.

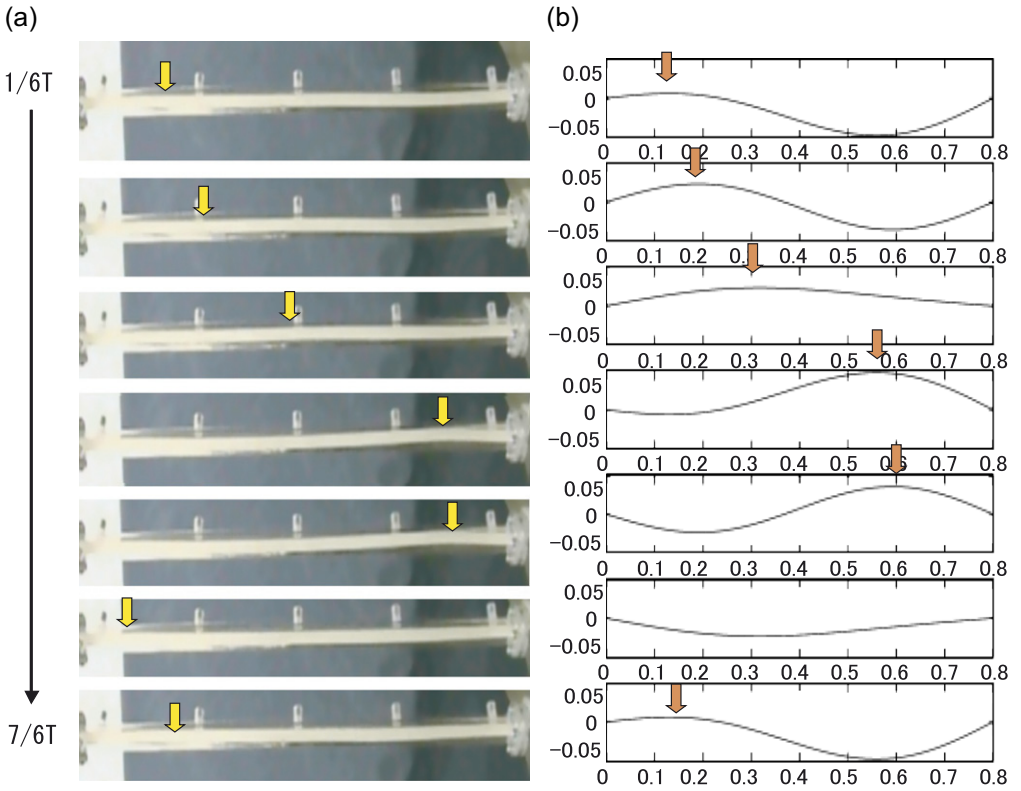

Fig. 12. Travel of the second mode shape over one period. (a) Experiment. (b) Simulation.

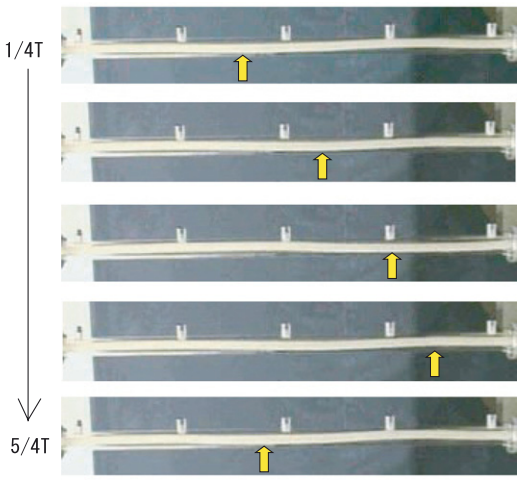

Fig. 13. Travel of the third mode shape over one period in experiment.

4.3. Energy balance due to traveling wave

In the vicinity of critical velocity, it is observed that the nodal point shifts in the axial direction in both the experiment and the numerical analysis.

The generation of the traveling wave upon the transition from the nth mode to the $(n+1)$th mode can be presumed to depend on the macroscopic imbalance of the kinetic and potential energies of the beam. As the flow velocity increases after the onset of flutter, the energy supplied to the beam by the fluid exceeds the energy consumed by the flutter through dissipation in the material, structural damping and fluid friction. Thus, the traveling wave is generated in order to keep the balance of energy. This mechanism can be explained by using the conveyance action due to the traveling wave of a vibration, as shown in Fig. 15.

Let us consider a leakage flow located on the surface of a beam vibrating with a traveling wave as shown in Fig. 15. That is, as a force is necessary to generate the distortion of vibration response in the axial direction, and also to generate

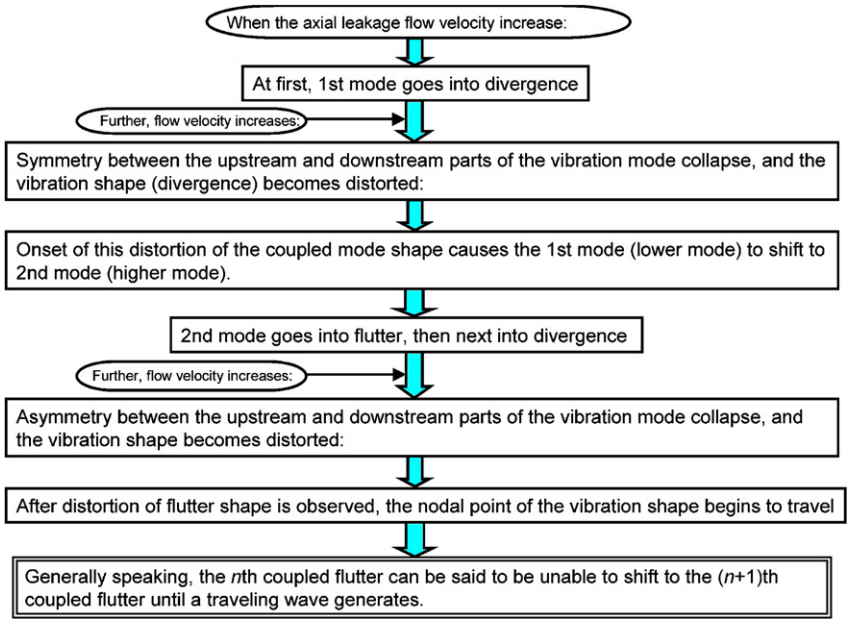

Fig. 14. Summary on mechanism of traveling wave generation.

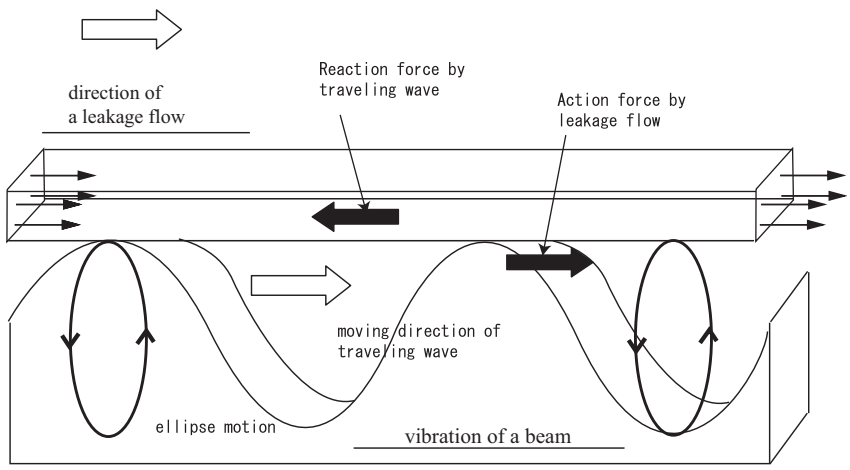

Fig. 15. Schematic illustration of a traveling wave.

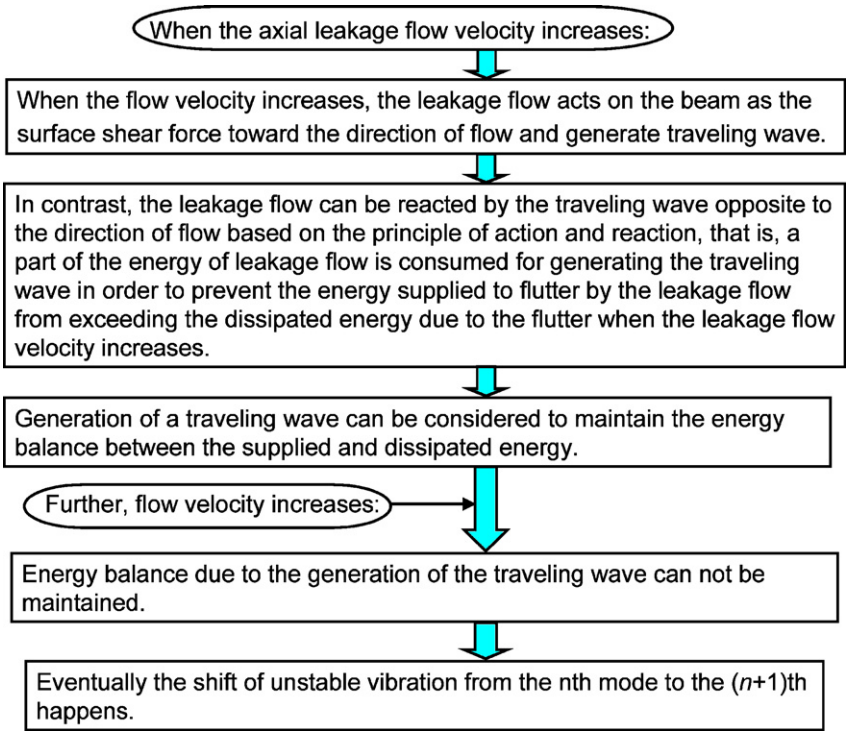

Fig. 16. Hypothesis of energy balance due to traveling wave.

the traveling wave, the steady and unsteady axial flow is considered to work on the structure for generating such force. When the flow velocity increases, the leakage flow acts on the beam as the surface shear force in the direction of flow and generates a traveling wave. In contrast, the leakage flow can be acted upon by the traveling wave, opposite to the direction of flow, based on the principle of action and reaction, that is, part of the energy of the leakage flow is consumed for generating the traveling wave in order to prevent the energy supplied to flutter by the leakage flow from exceeding the dissipated energy due to the flutter when the leakage flow velocity increases. From this point of view, the generation of a traveling wave can be considered necessary to maintain the energy balance between the supplied and dissipated energy. However, when the flow velocity increases further, the energy balance due to the generation of the traveling wave cannot be maintained, eventually resulting in the shift of unstable vibration from the nth to the $(n+1)$th unstable vibration. This mechanism of energy balance due to a traveling wave is summarized in Fig. 16.

5. Conclusions

The following conclusions have been reached.

(i) The unstable vibration behavior of an axisymmetric circular beam subjected to axial leakage flow was clarified experimentally and analytically. The measured threshold of instability is found to show comparatively good agreement with the analytical results from an engineering viewpoint, although they are based on linear theory assuming laminar flow.
(ii) In the experiment, when the divergence or flutter of a lower mode shifts to a higher mode, especially in the case of flutter, it is found that they always accompany the generation of traveling waves.
(iii) In the analysis, the dynamic pre- and post-instability behavior, that is the shifting from a lower mode to a higher with accompanying distortion of the vibration response in the axial direction and traveling waves, is found to be in fairly good agreement with experiments although the analysis is based on linear theory.
(iv) The hypothesis on the generating mechanism of traveling waves is proposed by observing pre- and post-instability phenomena experimentally and analytically. That is, it can be considered that, when the energy supplied to the

beam by the fluid flow exceeds the energy consumed by flutter with no accompanying traveling wave, a traveling wave is generated at first at the transition from a lower vibration to a higher one, in order to suppress the imbalance of energy; then the vibration shifts to the higher vibration as a higher vibration consumes more energy.

References

Arai, M., Tajima, K., 1997. Leakage-flow-induced vibrations of an axisymmetric body (theories and experiments on the stability of an axisymmetric body for one degree of freedom of rotational motion). Proceedings of Asia-Pacific Conference 97, 698–703.

Blevins, R.D., 1977. Flow-Induced Vibration. Van Nostrand Reinhold Company.

Chen, S.S., 1987. Flow-Induced Vibration of Circular Cylindrical Structures. Springer, Berlin.

Fujita, K., Ito, T., 1992. Study on leakage flow-induced vibration of an axisymmetric cylindrical rod due to axial flow. In: Proceedings of ASME Pressure Vessels and Piping Conference, vol. 244, pp. 33–43.

Fujita, K., Ito, T., Kawata, Y., Izumi, H., 1994. Axial leakage flow-induced vibration of a long flexible rod with small gaps. In: Proceedings of ASME Pressure Vessels and Piping Conference, vol. 273, pp. 133–143.

Fujita, K., Shintani, A., 2001. Axial leakage flow-induced vibration of the elastic rod as the axisymmetric continuous flexible beam. ASME Journal of Pressure Vessel Technology 123, 421–428.

Hobson, D.E., 1982. Fluid-elastic instabilities caused by flow in an annulus. Proceedings of third International Conference on Vibration in Nuclear Plant. Keswick, UK, pp. 440–461.

Inada, F., Hayama, S., 1990a. A study on leakage-flow-induced vibrations. Part 1: fluid-dynamic forces and moments acting on the walls of a narrow tapered passage. Journal of Fluids and Structures 4, 395–412.

Inada, F., Hayama, S., 1990b. A study on leakage-flow-induced vibrations. Part 2. stability analysis and experiments for 2-degree-of-freedom systems combining translational and rotational motions. Journal of Fluids and Structures 4, 413–428.

Païdoussis, M.P., 1998. Fluid-Structure Interactions: Slender Structures and Axial Flow, vol. 1. Academic Press, London.

Païdoussis, M.P., 2004. Fluid-structure Interactions: Slender Structures and Axial Flow, vol. 2. Elsevier, Academic Press, London.

Païdoussis, M.P., Mateescu, D., Sim, W.-G., 1990. Dynamics and stability of a flexible cylinder in a narrow coaxial cylindrical duct subjected to annular flow. Journal of Applied Mechanics 57, 232–240.

Yasuo, A., Païdoussis, M.P., 1989. Flow-induced instability of heat-exchanger tubes due to axial flow in a diffuser-shaped, loose intermediate support. ASME Journal of Pressure Vessel Technology 111, 428–434.